Oettinger, G., Haak, V., Larsen, J. C. (2001): Noise reduction in magnetotelluric time-series with a new signal–noise separation method and its application to a field experiment in the Saxonian Granulite Massif. - Geophysical Journal International, 146, 3, pp. 659—669.

DOI: http://doi.org/10.1046/j.1365-246X.2001.00473.x

Geophys. J. Int. (2001) **146,** 659–669

Noise reduction in magnetotelluric time-series with a new signal–noise separation method and its application to a field experiment in the Saxonian Granulite Massif

G. Oettinger,[1,*] V. Haak[1] and J. C. Larsen[2]

[1] *GeoForschungsZentrum, Telegrafenberg,* D-14473 *Potsdam, Germany. E-mail: vhaak@gfz-potsdam.de*
[2] *Pacific Marine Environmental Laboratory, National Oceanic and Atmospheric Administration, contribution* 2173, 7600 *Sand Point Way NE, Seattle* WA 98115-0070, *USA*

Accepted 2001 April 19. Received 2001 March 28; in original form 2000 March 10

SUMMARY

In the presence of large and continuous correlated noise signals in measured electric and magnetic time-series, even robust remote-reference methods give erroneous estimates of MT transfer functions. If clean remote time-series are available, it is possible to separate MT and correlated noise signals and to derive unbiased MT transfer functions with the signal–noise separation method (SNS) (Larsen *et al.* 1996). In practice, the remote time series also contain some noise and the results can be improved by using a second remote data set and the SNS-remote-reference technique. We tested this method with data from the Saxonian Granulite Massif (SGM), Germany, where strong correlated noise signals were detected. We used remote data which were recorded 350 km away and, for short periods, data from sites of the profile across the SGM itself (distance 5 km). To show the efficiency of the signal–noise separation we first determined a 'true' MT transfer function from time-series with low noise level. In a second step we reproduced the results from processing very noisy data sections. We were able to determine useful MT transfer functions even when the MT variations have less than 10 per cent share of the measured variations. We identified dominant noise in the measured time-series from pipelines and trains.

Key words: data processing, electromagnetic methods, electromagnetic noise, magnetotellurics.

1 INTRODUCTION

In highly industrialized areas magnetotelluric- (MT) induced variations are contaminated by strong manmade noise signals (Szarka 1988; Junge 1996; Banks 1998). Classic single-site processing methods are based on the assumption of noise-free data in either the electric or the magnetic channels and therefore give wrong MT transfer functions in the presence of correlated noise. Many techniques have been applied to solve this problem, in particular the remote-reference (RR) method (Gamble *et al.* 1979), which utilizes data from a remote second station and has been successfully used in many cases (Jones *et al.* 1989).

The RR method is improved by robust statistical techniques, using coherency-based criteria (Egbert & Booker 1986; Ritter *et al.* 1998), but this technique still gives erroneous results if strong correlated noise signals are present during most of the recording time. To deal with such kind of noise, Egbert (1997) used a so-called 'Robust Multivariate Errors in Variables' algorithm in order to calculate correlated and uncorrelated noise levels iteratively by using data from multiple stations. Another method was demonstrated by Larsen *et al.* (1996), who introduced a new method which we will call here the signal–noise separation (SNS) method. This method improves the signal-to-noise level by separating MT signals and correlated noise signals. The label 'SNS' means the separation of two types of signals, MT signals and industrial noise. The SNS method was tested with data from central Italy and remote reference time-series from an island 50 km west.

The critical point in the SNS method is the assumption of noise-free remote data. In this paper we avoid this problem by using two remote sites, combining SNS and RR into the SNS(RR) method. After describing the different processing methods, we present results from an MT campaign in the Saxonian Granulite Massif (Eastern Germany), where strong and continuous correlated noise signals were detected. To clean the data we used remote sites from the Odenwald region 350 km southwest of the measurement area. We focus on two period ranges: short periods from 0.1 to 5 s and long periods from 5 to 200 s. To test the efficiency of the signal–noise separation, we

* Now at: McKinsey & Company, Inc, Königsallee 60 C, D-40027 Düsseldorf, Germany.

chose example sites having data sections with very high noise level and with low noise level. We also show examples of time derivatives and identify some typical and dominant noise signals in Saxonia.

2 SIGNAL–NOISE SEPARATION METHOD

2.1 MT signals and noise signals

The fundamental observations at the Earth's surface are the electric time-series $\vec{e}(t)$ in mV km^{-1} and the magnetic time-series $\vec{b}(t)$ in nT. Their Fourier transforms are $\vec{E}$ and $\vec{B}$. Under the condition of quasi-uniform fields, the relation between the electric and magnetic signals can be written

$$\begin{pmatrix} E_x \\ E_y \end{pmatrix} = \begin{pmatrix} Z_{xx} & Z_{xy} \\ Z_{yx} & Z_{yy} \end{pmatrix} \begin{pmatrix} B_x \\ B_y \end{pmatrix}, \tag{1}$$

with the short version $\vec{E} = \mathbf{Z}\vec{B}$ where Z_{ij} are the components of the complex valued transfer function tensor $\mathbf{Z}$. Cartesian coordinate systems x, y and z are defined to be positive when pointing towards the north, the east and downwards, respectively. $\mathbf{Z}$ is usually plotted as apparent resistivity

$$\rho_{a_{ij}} = 0.2T\left|Z_{ij}\right|^2,\ i,j \in \{x, y\} \tag{2}$$

and phase

$$\varphi_{ij} = \arctan\left(\frac{\mathrm{Im}Z_{ij}}{\mathrm{Re}Z_{ij}}\right) \tag{3}$$

over the period T.

Not all signals that are measured at the Earth's surface include usable information about the distribution of the electrical conductivity at depth. Particularly in very industrialized regions it is necessary to differentiate between MT signals produced by ionospheric and magnetospheric sources and the noise signals produced by near-by environmental (manmade) sources.

For eq. (1) to be valid it is necessary that the magnetic field be quasi-homogeneous, i.e. homogeneous over a distance larger than the penetration depth. All other parts of the measured electric and magnetic fields are considered as noise contributing signals because they do not fulfill that requirement. Additionally disturbances from the instruments themselves and geochemical variations of the electrode-soil system will exist. We can subdivide the noise signals into correlated noise (CN) where the noise is coherent between $\vec{E}$ and $\vec{B}$ channels and uncorrelated noise (UN). With this subdivision we can describe the fields $\vec{E}$ and $\vec{B}$ as a sum of three parts:

$$\begin{aligned} \vec{E} &= \vec{E}^{MT} + \vec{E}^{CN} + \vec{E}^{UN} \\ \vec{B} &= \vec{B}^{MT} + \vec{B}^{CN} + \vec{B}^{UN} \end{aligned} \tag{4}$$

The correlated noise originates from the near-field of controlled electric and magnetic sources and causes distortion and scatter of the apparent resistivity and phase curves. Most noise signals of this type are caused by earthing currents of technical equipment, e.g., electrified railways, corrosion prevention in pipelines by electrical means, mining machines, electric cables or pasture fences. Comprehensive lists can be found in Szarka (1988) and Junge (1996).

Many noise signals can be attributed to the near-field of a grounded electric dipole. Zonge & Hughes (1987) describe the EM fields of a horizontal electric dipole grounded in a homogeneous halfspace (Fig. 1). Two cases can be considered, the near-field case and the far-field case. The near-field case applies when the separation between transmitter and receiver is smaller than the depth of penetration ($r_A \ll \delta$), with $\delta = \sqrt{2/\omega\mu_o\sigma}$, where ω = frequency, μ_o = free space magnetic permeability, σ = electrical conductivity of half-space. $\vec{E}$ and $\vec{B}$ vary as $1/r^3$ and $1/r^2$ respectively, both independently of frequency. The apparent resistivity at a fixed site is according to eq. (2) directly proportional to the period T in a logarithmic scale. This effect produces the artificial 45° rise of the apparent resistivity curves. The phase according to eq. (3) is zero for all

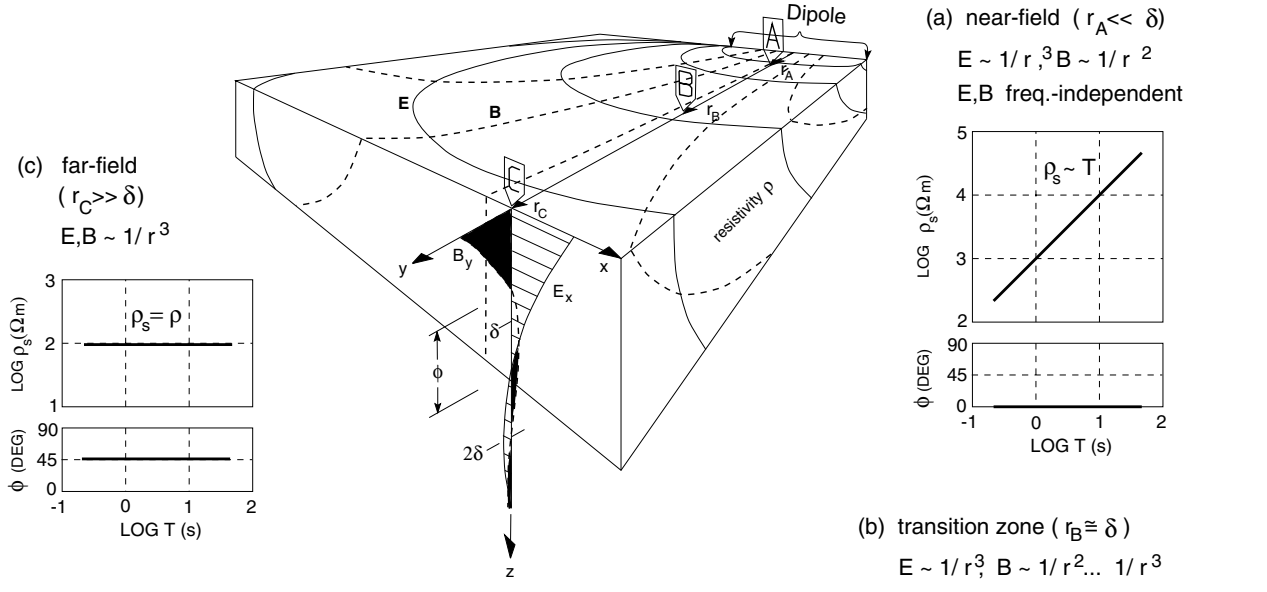

Figure 1. Diagrammatic sketch of the EM field propagation in a homogeneous half-space (modified after Zonge & Hughes 1987). MT measurement in three zones from an electric dipole, with δ = depth of penetration in a uniformly conducting halfspace: (a) Near-field ($r_A \ll \delta$); (b) Near-field/far-field transition zone ($r_B \approx \delta$); (c) Far-field ($r_A \gg \delta$).

periods. The change of the ratio $\vec{E}/\vec{B}$ in any lateral distance at a fixed period goes with $1/r$, the separation distance between transmitter and receiver, due to the different dependencies of the electric and magnetic field from distance. With this it becomes clear that dipole fields produced in the neighbourhood of the receiver dominate the electric variations (uncorrelated noise) and not the magnetic variations and therefore appear as UN. This corresponds to the common observation that in industrialized areas the electric fields are much more contaminated by noise than the magnetic fields. Therefore the electric dipole model seems to be useful to describe most noise signals.

In the near-field/far-field transition zone ($r_B \approx \delta$), $\vec{B}$ varies as $1/r^2$ to $1/r^3$ and the apparent resistivity depends on geometry, frequency and resistivity.

In the far-field ($r_A \gg \delta$), $\vec{E}$ and $\vec{B}$ decay as $1/r^3$ and the apparent resistivity depends on frequency and resistivity. The ratio $\vec{E}/\vec{B}$ is independent of the separation r from the dipole source. The phase difference between $\vec{E}$ and $\vec{B}$ (eq. 3) is 45° (homogeneous earth phase response) and the apparent resistivity (eq. 2) is the resistivity of the half-space.

From these considerations of a grounded electric dipole it is clear that the near field and transition zone terms of electric and magnetic fields produce that part of the measured field which causes scatter and distortion. Since it is also the most inhomogeneous part of the field, the inhomogeneity may be used to separate the MT signal from the correlated noise, while the uncorrelated noise will be treated by well known least squares and remote reference techniques. The far fields of industrial noise will approach the MT assumption of quasi-homogeneous fields and will therefore be included as part of the MT signal.

2.2 Transfer function estimation

2.2.1 *Least-square method (LS)*

The starting point for determining the transfer function $\mathbf{Z}$ is the MT basic eq. (1). We have n time series segments with data from two magnetic and two electric channels and we want to determine $\mathbf{Z}$ for m narrow frequency bands. For the LS method we assume two noise-free input channels, which are usually the magnetic variations. For the north-component of the electric field we obtain the following system of equations with two unknowns:

$$\begin{pmatrix} E_{x1} \\ \vdots \\ E_{xN} \end{pmatrix} = \begin{pmatrix} B_{x1} & B_{y1} \\ \vdots & \vdots \\ B_{xN} & B_{yN} \end{pmatrix} \begin{pmatrix} Z_{xx} \\ Z_{xy} \end{pmatrix} + \begin{pmatrix} R_{x1} \\ \vdots \\ R_{xN} \end{pmatrix}. \tag{5}$$

$N = n \times m$ and with the notation $\mathbf{E}_x$ as numerical column vector, $\mathbf{B} = (\mathbf{B}_x, \mathbf{B}_y)$ as numerical tensor with the two subcolumn vectors $\mathbf{B}_x$ and $\mathbf{B}_y$. This notation thus discriminates between physical vectors as $\vec{E}$ (e.g. in the short version of eq. 1) and numerical vectors as $\mathbf{E}_x$. The column vector $\mathbf{Z}_x$ relates to the transfer function tensor by $\mathbf{Z} = (\mathbf{Z}_x, \mathbf{Z}_y)^T$. The short version of eq. (5) is thus

$$\mathbf{E}_x = \mathbf{B}\mathbf{Z}_x + \mathbf{R}_x . \tag{6}$$

The residual $\mathbf{R}_x$ represents the uncorrelated noise in the electric variations. Normally the impedances are estimated by minimizing the electric residual $\Sigma_i |R_{xi}|^2 \rightarrow$ minimum (Sims *et al.* 1971 least-squares technique). From this we obtain the following relationship:

$$\mathbf{Z}_x = (\mathbf{B}^\dagger \mathbf{B})^{-1} (\mathbf{B}^\dagger \mathbf{E}_x) \tag{7}$$

($\dagger$ = Hermitian transpose), or in detail for the Z_{xy} component:

$$Z_{xy} = \frac{[E_x B_y^*][B_x B_x^*] - [E_x B_x^*][B_x B_y^*]}{[B_x B_x^*][B_y B_y^*] - [B_x B_y^*][B_y B_x^*]} \tag{8}$$

([...] = stack over segments and frequencies in one band, * = conjugate complex).

Analogous relations hold for the y-component: $\mathbf{E}_y = \mathbf{B}\,\mathbf{Z}_y + \mathbf{R}_y$ and

$$\mathbf{Z}_y = (\mathbf{B}^\dagger\, \mathbf{B})^{-1}\, (\mathbf{B}^\dagger\, \mathbf{E}_y) . \tag{9}$$

In the following we will restrict our considerations to the x-component. In practice, measured data also includes noise in the magnetic variations. When estimating $\mathbf{Z}$ according to eq. (7), noise in the magnetic variations yields bias which cannot be neglected. The bias is caused by increased power spectra $[B_i B_i^*]$ ($i \in \{x, y\}$) in the denominator of eq. (8). The resistivity values are biased downwards (Goubau *et al.* 1978). Under special circumstances it is possible to compensate bias without remote data (Müller 2000).

2.2.2 *Remote-reference (RR) method*

A reliable method to avoid bias is the RR technique (Gamble *et al.* 1979). This method requires synchronized field variations (e.g. magnetic variations $\vec{B}_r$) which are recorded at a clean remote site. For middle latitudes the variations and pulsations of the magnetotelluric source field are well correlated over some 100 km (Schmucker 1984), and therefore the remote site can be farther than 100 km away from the local site.

For the case of quasi-uniform fields, the local electric field $\vec{E}$ and the remote magnetic field $\vec{B}_r$ are related by the linear, time-independent transfer function $\mathbf{Z}_r$: In tensor notation: $\mathbf{E} = \mathbf{Z}_r \mathbf{B}_r$. This relation between the numerical field vectors of the physical E_x-component and the magnetic field is: $\mathbf{E}_x = \mathbf{B}_r \mathbf{Z}_{xr} + \mathbf{R}_{xr}$ which in detail reads

$$\begin{pmatrix} E_{x1} \\ \vdots \\ E_{xN} \end{pmatrix} = \begin{pmatrix} B_{x1r} & B_{y1r} \\ \vdots & \vdots \\ B_{xNr} & B_{yNr} \end{pmatrix} \begin{pmatrix} Z_{xxr} \\ Z_{xyr} \end{pmatrix} + \begin{pmatrix} R_{x1r} \\ \vdots \\ R_{xNr} \end{pmatrix}. \tag{10}$$

The impedances are estimated by minimizing the electric residuals

$$\sum_i R_{xi} R_{xir}^* \tag{11}$$

by setting the derivatives with respect to $\mathbf{Z}_{rx}$ to zero and obtaining (instead of eq. 7)

$$\mathbf{Z}_x^r = (\mathbf{B}_r^\dagger\, \mathbf{B})^{-1}\, (\mathbf{B}_r^\dagger\, \mathbf{E}_x) , \tag{12}$$

where we define the tensor estimated by the RR method with $\mathbf{Z}^r$ (with the elevated index r) or in detail for the Z_{xy}^r component:

$$Z_{xy}^r = \frac{[E_x B_{yr}^*][B_x B_{xr}^*] - [E_x B_{xr}^*][B_x B_{yr}^*]}{[B_x B_{xr}^*][B_y B_{yr}^*] - [B_x B_{yr}^*][B_y B_{xr}^*]} . \tag{13}$$

Eqs (12) and (13) contain no autopowers, but crosspower spectra with the form $[B_i B_{ir}^*]$ between local fields and fields at the remote location.

Within the RR method the influence of CN signals is minimized by using robust procedures which work mostly by downweighting or rejecting noisy data sections (e.g. Egbert & Booker 1986; Chave & Thomson 1989; Larsen *et al.* 1996; Ritter *et al.* 1998). Robust techniques generate unbiased MT transfer functions, even if some segments are contaminated by correlated noise.

2.2.3 Signal–noise separation least squares SNS(LS) method

If most or all time-series contain correlated noise, even the RR method yields wrong estimates of the MT transfer function. In this case one possibility for deriving non-biased transfer functions is to separate MT and noise signals in the input channels with the aid of remote data. This technique was introduced by Larsen *et al.* (1996) and will be called here the signal–noise separation (SNS) method. The designation signal–noise separation symbolizes the division of all signal sources into two groups depending on whether the MT station is located in the near field or in the far field of one specific source. Generally the near-field part is a combination of all noise signals which are produced by different technical equipment near the MT location.

The first step in the SNS method is to separate the measured magnetic variations into MT signals and noise signals. For this we need remote data from a clean remote site in order to estimate the separation tensor **T**. We assume noise-free remote magnetic variations $\mathbf{B}_r$ and noisy local magnetic variations **B**. For the north component we get the relationship $\mathbf{B}_x = \mathbf{B}_r \mathbf{T}_x + \mathbf{R}_x$ or in detail:

$$\begin{pmatrix} B_{x1} \\ \vdots \\ B_{xN} \end{pmatrix} = \begin{pmatrix} B_{x1r} & B_{y1r} \\ \vdots & \vdots \\ B_{xNr} & B_{yNr} \end{pmatrix} \begin{pmatrix} T_{xx} \\ T_{xy} \end{pmatrix} + \begin{pmatrix} R_{x1} \\ \vdots \\ R_{xN} \end{pmatrix}. \tag{14}$$

For homogeneous source fields and a horizontal layered earth, **T** is unity. However, lateral conductivity anomalies cause anomalous horizontal magnetic fields on top of the source field. Thus **T** is generally frequency dependent, complex-valued and different from unity (Larsen *et al.* 1996).

The residual $\mathbf{R}_x$ represents the uncorrelated noise in the local magnetic variations. The least squares minimizing condition $\Sigma_i |R_{xi}|^2 \rightarrow$ minimum leads to the following relationship to estimate $\mathbf{T}_x$:

$$\mathbf{T}_x = (\mathbf{B}_r^\dagger \mathbf{B}_r)^{-1} (\mathbf{B}_r^\dagger \mathbf{B}_x). \tag{15}$$

Because the noise signals are not included in the remote magnetic variations, signal–noise separation can be done by treating **R** as a CN signal plus UN, thus $\vec{B}^{CU} = \vec{B}^{CN} + \vec{B}^{UN}$. We can subdivide the local magnetic variations into two parts:

$$\vec{B}^{MT} = \mathbf{T}\vec{B}_r \tag{16}$$

and

$$\begin{aligned} \vec{B}^{CU} &= \vec{B} - \vec{B}^{MT} \\ &= \vec{B} - \mathbf{T}\vec{B}_r . \end{aligned} \tag{17}$$

T is called the separation tensor because with **T** both parts of $\vec{B}$ can be determined subsequently from independent measurements of $B(\vec{t})$ and $B_r(\vec{t})$. With this separation we will now expand eq. (1) with the term $\vec{E}^{CN} = \mathbf{Z}^{CN}\vec{B}^{CN}$ and obtain the SNS equation

$$\begin{aligned} \vec{E}(\omega) &= \vec{E}(\omega)^{MT} + \vec{E}(\omega)^{CN} + \vec{E}^{UN} \\ &= \mathbf{Z}^{MT}(\omega)\vec{B}^{MT}(\omega) + \mathbf{Z}^{CN}(\omega)\vec{B}^{CN}(\omega) + \vec{E}^{UN} \\ &= \mathbf{Z}^{MT}(\omega)\vec{B}^{MT}(\omega) + \mathbf{Z}^{CN}(\omega)\vec{B}^{CN}(\omega) \\ &\quad + \mathbf{Z}^{CN}(\omega)\vec{B}^{UN}(\omega) - \mathbf{Z}^{CN}(\omega)\vec{B}^{UN}(\omega) + \vec{E}^{UN} \\ &= \mathbf{Z}^{MT}(\omega)\vec{B}^{MT}(\omega) + \mathbf{Z}^{CN}(\omega)\vec{B}^{CU}(\omega) + \vec{R}, \end{aligned} \tag{18}$$

where $\vec{R} = \vec{E}^{UN} - \mathbf{Z}^{CN}\vec{B}^{UN}$.

With eq. (18) one can estimate $\mathbf{Z}^{MT}$ and $\mathbf{Z}^{CN}$ simultaneously using least-squares, by solving a system of N equations:

$$\begin{pmatrix} E_{x1} \\ \vdots \\ E_{xN} \end{pmatrix} = \begin{pmatrix} B_{x1}^{MT} & B_{y1}^{MT} & B_{x1}^{CU} & B_{y1}^{CU} \\ \vdots & \vdots & \vdots & \vdots \\ B_{xN}^{MT} & B_{yN}^{MT} & B_{xN}^{CU} & B_{yN}^{CU} \end{pmatrix} \begin{pmatrix} Z_{xx}^{MT} \\ Z_{xy}^{MT} \\ Z_{xx}^{CN} \\ Z_{xy}^{CN} \end{pmatrix} + \begin{pmatrix} R_{x1} \\ \vdots \\ R_{xN} \end{pmatrix}. \tag{19}$$

In tensor short notation this numerical relation reads:

$$\mathbf{E}_x = \left(\mathbf{B}^{MT}\mathbf{B}^{CU}\right)\left(\mathbf{Z}_x^{MT}\mathbf{Z}_x^{CN}\right)^T + \mathbf{R}_x = \underline{\mathbf{B}}\underline{\mathbf{Z}}_x^T + \mathbf{R}_x . \tag{20}$$

Analogous to the LS method (eq. 7) we can estimate $\mathbf{Z}_x$ with the minimizing condition $\Sigma_i |R_{xi}|^2 \rightarrow$ minimum:

$$\underline{\mathbf{Z}}_x = (\underline{\mathbf{B}}^\dagger \underline{\mathbf{B}})^{-1} (\underline{\mathbf{B}}^\dagger \mathbf{E}_x), \tag{21}$$

where $\underline{\mathbf{Z}}_x$ is a tensor that combines $\mathbf{Z}_x^{MT}$ and $\mathbf{Z}_x^{CN}$ and $\underline{\mathbf{B}}$ combines $\mathbf{B}^{MT}$ and $\mathbf{B}^{CU}$ where underlining represents the combination.

Note: the use of the LS methods is valid only in the case of Gaussian noise. If non-Gaussian noise exists, robust procedures must be included. The algorithms developed in this study are part of the robust iterative procedures used and described in detail (time-series preprocessing, correction for outliers, calculation of confidence limits, rotation of magnetic time-series, estimation of smooth transfer function) by Larsen *et al.* (1996).

2.2.4 Signal–noise separation remote-reference method SNS(RR)

To estimate unbiased magnetotelluric transfer functions with the SNS method requires noise-free remote magnetic variations. However, sufficiently accurate remote data is often not available. Noise in the remote channels increases the autopower spectra $[\mathbf{B}_r^\dagger \mathbf{B}_r]$ in eq. (15) and gives biased impedances. In highly industrialized areas it is normally impossible to find a remote location which delivers noise-free magnetic time-series for all periods of interest and during the whole measurement campaign. In this case a second remote field $\mathbf{B}_{r2}$ (or $\mathbf{E}_r$) can be used to estimate all transfer functions **T** and **Z** with the RR technique. To express the two methods apart, we label them SNS(LS-LS) and SNS(RR-RR). With the second remote field $\mathbf{B}_{r2}$ we have two relationships $\vec{B} = \mathbf{T}\vec{B}_r$ and $\vec{B} = \mathbf{T}_2\vec{B}_{r2}$. Using the

remote reference method we can estimate two separation transfer functions

$$\mathbf{T}_x = (\mathbf{B}_{r2}^{\dagger}\mathbf{B}_r)^{-1}(\mathbf{B}_{r2}^{\dagger}\mathbf{B}_x) \qquad \text{and}$$
$$\mathbf{T}_{x2} = (\mathbf{B}_r^{\dagger}\mathbf{B}_{r2})^{-1}(\mathbf{B}_r^{\dagger}\mathbf{B}_x)\,. \tag{22}$$

Using either $\mathbf{T}_x$ or $\mathbf{T}_{x2}$ we get the SNS(RR-RR) equations

$$\mathbf{E}_x(\omega) = \underline{\mathbf{B}}(\omega)\underline{\mathbf{Z}}_x(\omega) + \mathbf{R}_x \qquad \text{and}$$
$$\mathbf{E}_x(\omega) = \underline{\mathbf{B}}_2(\omega)\underline{\mathbf{Z}}_{2x}(\omega) + \mathbf{R}_{2x} \tag{23}$$

with the following solutions:

$$\underline{\mathbf{Z}}_x = (\underline{\mathbf{B}}_2^{\dagger}\underline{\mathbf{B}})^{-1}(\underline{\mathbf{B}}_2^{\dagger}\mathbf{E}_x)\,,$$
$$\underline{\mathbf{Z}}_{2x} = (\underline{\mathbf{B}}^{\dagger}\underline{\mathbf{B}}_2)^{-1}(\underline{\mathbf{B}}^{\dagger}\mathbf{E}_x)\,, \tag{24}$$

where, again, the underlining represents the combination of $\mathbf{Z}_x^{MT}$ and $\mathbf{Z}_x^{CN}$. It is sensible to select either $\underline{\mathbf{Z}}_x$ or $\underline{\mathbf{Z}}_{2x}$ depending on which has the smallest residual variance $\Sigma_i |R_{xi}|^2$ or $\Sigma_i |R_{xi2}|^2$.

Because of increased confidence limits for RR estimates (Schmucker 1984), the transfer function estimates may be unstable if one of the remote sites is substantially more noisy. In this case it is often sufficient to estimate $\mathbf{T}$ with RR method (eq. 22), but to adopt the least-squares solution (eq. 21) for the subsequent estimation of $\mathbf{Z}$ using the least noisy remote site. We label this method SNS(RR-LS). All methods used in this paper are summarized in Table 1.

Because the CN transfer function $\mathbf{Z}^{CN}$ is estimated separately, the SNS method gives the interesting opportunity to study the noise signals which occur in the measured time-series. Note that $\mathbf{Z}^{CN}$ represents an averaged transfer function for all noise sources. However, if one noise signal is dominant in amplitude and intensity, $\mathbf{Z}^{CN}$ describes the transfer characteristics of this special noise source and is well determined. In this case the other CN signals remain in the residual.

For more information concerning the robust iterative procedure (time-series pre-processing, correction for outliers, calculation of confidence limits, rotation of magnetic time-series, estimation of smooth transfer function) see Larsen *et al.* (1996).

3 SURVEY DESIGN

The field data were recorded in 1995 along the profile 'Granu95-A' in Saxonia, Germany. The MT survey crosses the Saxonian Granulite Massif north of Chemnitz and was carried out to study the deeper structure of the Saxo-Thuringian Terrane. For modelling results and interdisciplinary interpretation see DEKORP & Orogenic Processes Working Groups (1999), Krawczyk *et al.* (1999) and Oettinger (1999).

To discuss the application of the methods described in this paper we concentrate on some sites in the region of the exposed Saxonian Granulites in the central part of the profile Granu95-A. The site locations are shown in Fig. 2. The area is highly industrialized (Chemnitz area, electrified railways, mining area) and the underground is highly resistive, which means that noise signals have large-scale influence. The site separation

Table 1. Table of processing methods. 1-site = single-site equation (Eq. 1), 2(3)-site = two(three)-sites equation (Eq. 18 resp. 23).

Method		Number of MT sites	Remote ref.-fields
Single Site	SS	1-site	0
Remote-reference	RR	2-site	1
Signal-separation	SNS(LS-LS)	2-site	1
Sign.-sep. rem.-ref. (only T)	SNS(RR-LS)	3-site	2
Sign.-sep. remote-reference	SNS(RR-RR)	3-site	2

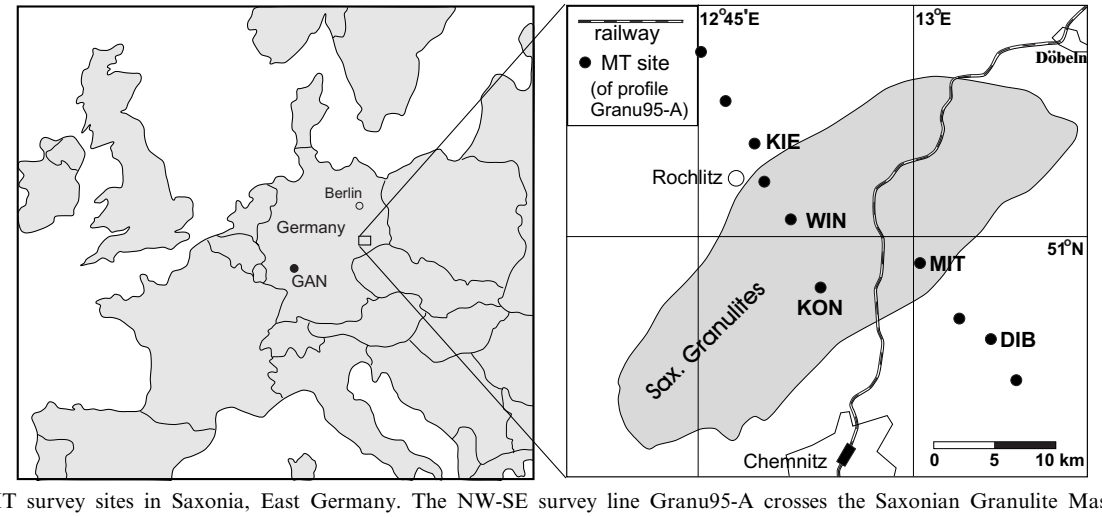

Figure 2. MT survey sites in Saxonia, East Germany. The NW-SE survey line Granu95-A crosses the Saxonian Granulite Massif (shaded). The electrified railway Chemnitz-Döbeln runs through the measurement area.The remote site GAM is located in the Odenwald, 350 km SW of the survey line.

is 4–10 km and the data were recorded continuously with a sampling rate of 20 Hz. A rough estimation on a reliable distance for remote sites can be done on the basis of the dipole model (Fig. 1) by determining which minimum distances between dipole, local and remote site should be kept to identify the inhomogenous dipole field. In accordance with the high resistive rocks in the Granulite Massif, Oettinger (1999) shows that sites from the profile Granu95-A itself can only be used as reference for periods less than 5 s. For longer periods up to 200 s remote time-series recorded several hundred kilometres away are required. For this we used data from a simultaneous MT campaign in the Odenwald, 350 km south-west of the line Granu95-A (see Fig. 2). The Odenwald survey is described in Michel & Tezkan (1996) and Michel (1997). At Odenwald site GAN we found a low noise-level during most of the recording time and so this site was adopted as the remote location.

4 SIGNAL–NOISE SEPARATION FOR PERIODS OF LESS THAN 5 s

In this section, we present data from site WIN, located in the region of the exposed Saxonian granulites (see Fig. 2). We focus on the period range between 0.1 and 5 s. For these periods we can use remote sites either from the profile Granu95-A itself or from the Odenwald survey 350 km to the south-east. We concentrate on the easterly component of the electric variations and on the transfer function Z_{yx}. At site WIN we found time-series with both low noise level and a very high noise level. First we show results of processing derived from time-series with low noise level to give a well-determined 'true' MT transfer function. Second, we reproduce the 'true' function by processing very noisy time-series and show the results in the time domain. Before starting the robust processing of the two different time intervals, we subdivided the data into non-overlapping sections with a fixed length of 256 data points (time-series length 12.8 s) and removed linear trends and large spikes.

4.1 Low noise level

At location WIN we have time-series with relatively low noise level on October 10, 1995, 2:00–2:45 GMT. We subdivided the data in 210 sections and used magnetic remote data from sites GAN (350 km away) and KON (6.5 km away).

The processing results are shown in Fig. 3. Considering the LS results on a single site (Fig. 3a), the resistivity and phase values are not consistent. This can easily be seen from the phase-jump at the period of 1 s. This bias is presumably caused by some CN signals, but is completely compensated when using the RR method (Fig. 3b,c). In this connection, both remote sites GAN (Fig. 3b) and KON (Fig. 3c) are suitable.

The signal–noise separation of the measured magnetic variations is very important for the quality of the SNS results, which means in this case the estimation of the separation tensor elements T_{xx} and T_{xy}. Of these two elements T_{xx} is more important, because **T** is normally approximately unity. In this and all following examples the amplitude of T_{xy} is lower than 0.1 and is not shown here.

Fig. 4 shows three different estimates of T_{xx}. Fig. 4(a) gives the north separation transfer function between the sites WIN and GAN, Figs 4(b) and (c) between sites WIN and KON, where the results in Fig. 4(c) are estimated with the RR method (second remote site GAN). The curves are approximately flat and well derived, especially with RR method (Fig. 4c). The coherency squared between measured and predicted variations is 0.77, 0.93 and 0.95, respectively. The phase goes through a change of about -90° from the shortest to the longest periods, which is related to timing problems (Oettinger 1999). However, this is immaterial for estimating the time-series at site WIN, because the time-shift is small and mathematically exactly described.

With the signal separation based on the three functions given in Fig. 4 we get the transfer functions shown in Fig. 3(d) and (e). Dots show MT transfer functions Z_{yx}^{MT} and open circles

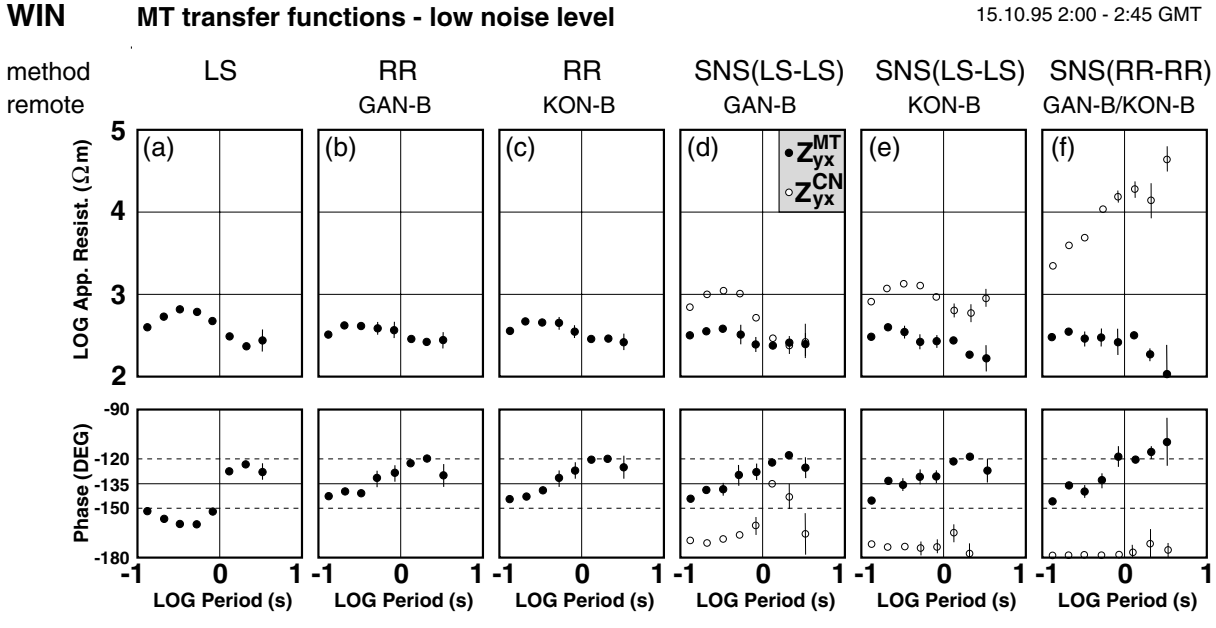

Figure 3. Different estimates of the MT transfer function Z_{yx}^{MT} (dots) and the CN transfer function Z_{yx}^{CN} (open circles) at site WIN, derived from 210 time-series with relatively low noise level. (a) LS method, (b) RR method, (d) SNS(LS-LS) method, (f) SNS(RR-RR) method. Remote sites: GAN (350 km away) and KON (6.5 km away).

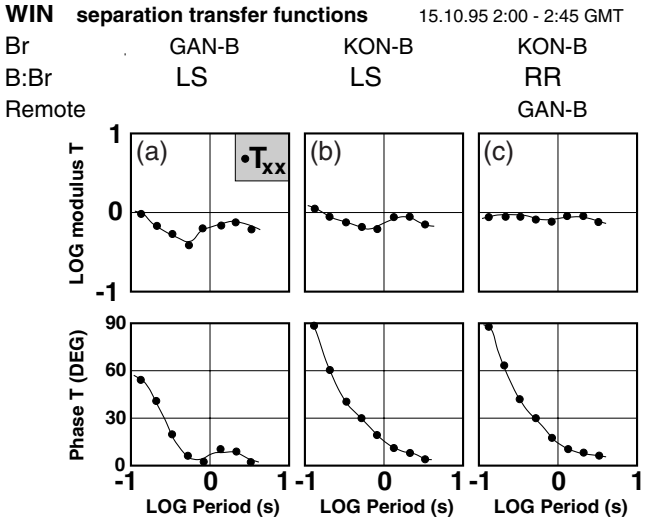

Figure 4. Separation transfer functions T_{xx} between the north component of the magnetic time-series at site WIN and remote site GAN (a) and KON (b). In (c), T_{xx} is estimated with the RR method (second remote site GAN). Dots represent band-averaged values and the curves smooth transfer functions. The unusual phase curve is caused by problems with time synchronization.

CN transfer functions Z_{yx}^{MT}. The MT transfer functions confirm the RR results (Fig. 3b,c). Using remote site GAN (Fig. 3d) or KON (Fig. 3e) gives comparably good results. The SNS(RR-RR) method (Fig. 3f) yields the same results, but with some larger errors.

The CN functions (open circles) have small phases near -180° and high resistivity values compared to the MT resistivities. In contrast to the SNS results (Fig. 3d,e), the CN resistivity values estimated with the SNS(RR-RR) method (Fig. 3f) increase directly proportional with the period. This characteristic in connection with small phases is typical for MT measurements in the near-field of an electric dipole. Therefore we assume that the dominant noise signals in such time-series can be described with the near-field model of an electric dipole. The values estimated with the SNS(LS-LS) method are obviously biased downwards for long periods by uncorrelated noise in the remote channels. Therefore, in this example the SNS(RR-RR) method gives better results for Z_{yx}^{CN} than the SNS(LS-LS) method.

For SNS(RR-RR) estimates, the partial coherence-squared between the electric and MT magnetic variations is 0.35, while the partial coherence-squared is 0.28 between the electric and the CN magnetic variations. This means there is 37 per cent uncorrelated noise. For SNS estimates the values are similar.

With the exception of the LS-single site estimates, all methods give comparable transfer functions of good quality. From the functions shown in Fig. 3(b) and (f) we calculated an averaged, 'true' transfer function. In the next section we will reproduce the 'true' function from analyzing very noisy time-series.

4.2 High noise level

As an example of a very noisy time-series we discuss data from Oct. 18th 1995, 22:00–23:04 GMT (300 sections). We used magnetic remote data from sites GAN (350 km away) and MIT (12 km away). The affiliated separation tensor elements T_{xx} are as well determined as the functions given in Fig. 4 and they are not shown here.

The results from the different processing methods are given in Fig. 5. Compared to the 'true' curves (dashed line) the LS method (Fig. 5a) and the RR method (Fig. 5b,c) give wrong results (resistivities overestimated, phases underestimated). The 'true' transfer function is only reproduced correctly with the SNS(LS-LS) method (Fig. 5d,e) and SS(RR-RR) method (Fig. 5f), although with some larger errors especially for the SNS(RR-RR) results. For SNS(RR-RR) estimates the partial coherence-squared is 0.25 between the electric and MT magnetic variations and 0.34 between the electric and CN magnetic variations. For long periods, the SNS(RR-RR) method once

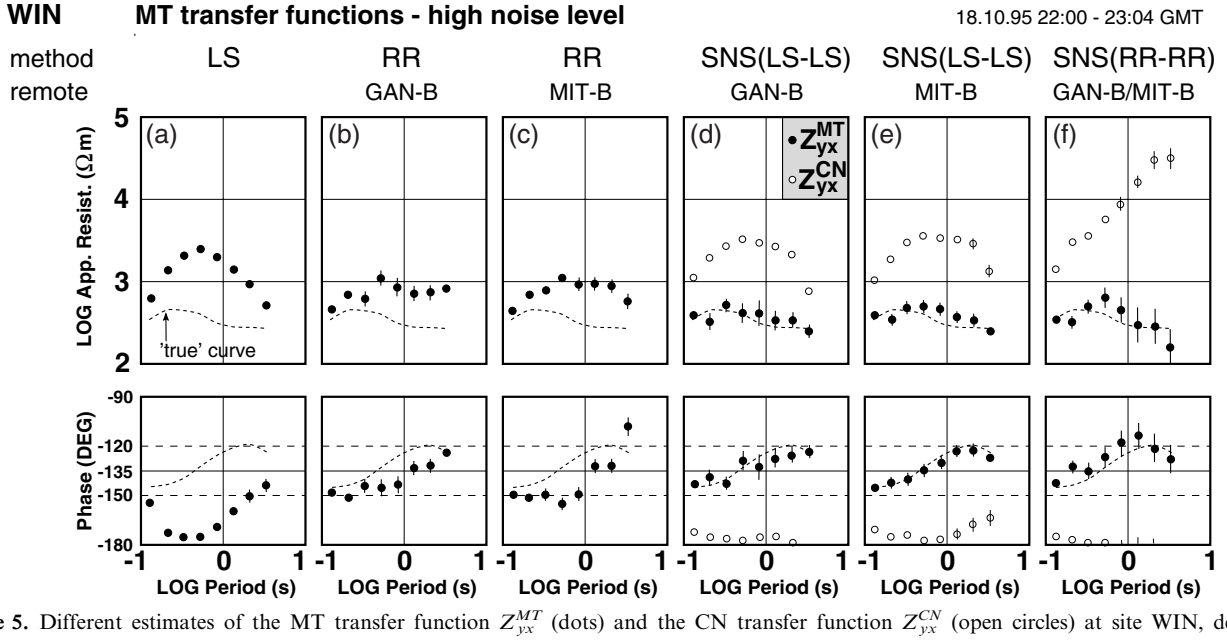

Figure 5. Different estimates of the MT transfer function Z_{yx}^{MT} (dots) and the CN transfer function Z_{yx}^{CN} (open circles) at site WIN, derived from 300 time-series with high noise level. (a) LS method, (b) (RR method, (d) SNS(LS-LS) method, (f) SNS(RR-RR) method. Remote sites: GAN (350 km away) and MIT (12 km away). The dashed curve shows the 'true' transfer function from Fig. 3

more facilitates a more accurate signal separation than the SNS(LS-LS) method (rising CN resistivities over the period). Correlated noise in the WIN time-series might arise from agricultural equipment on farms close to the site location, plants in the town Rochlitz (5 km to the northeast) and a NS running railway (7 km east).

Time series of the MT and CN variations are given in Fig. 6 for one section. Apart from periods of about 2 s, the MT variations have small periods less than 0.2 s, which can be interpreted as Schumann resonances (e.g. Polk 1982). The CN electric variations and the residual have larger amplitudes than the MT electric variations. There are no correlations between the two magnetic or the three electric time-series, which is a good sign for a successful signal separation.

The CN electric and magnetic variations are of similar apperance, which indicates that the CN transfer function is approximately a constant with 0° phase (-180° phase without inverting of magnetic channels, respectively). The spikes at the timemarks of 1.5 and 4.5 seconds (circled 1 in Fig. 6) are probably caused by corrosion protection inspection measurements along a pipeline. A test voltage is switched on for typically 3 s and then switched off for a longer time interval (typically 12 or 27 s). In the next section we present time-series with very strong pipeline noise. The CN time-series of the site WIN and the neighbouring sites are only slightly correlated for periods less than 5 s (Oettinger 1999).

4.3 Very high noise level: pipeline noise

Normally, natural gas pipelines are operated with a constant voltage (for protection from corrosion) which has low influence on MT measurements. However, the synthetic substance surrounding the pipelines is inspected at regular intervals. For these inspections, large test voltages in rectangular form are applied to the pipelines. The signals from switching on and off the test voltage can be observed in MT time-series some tens of kilometres away.

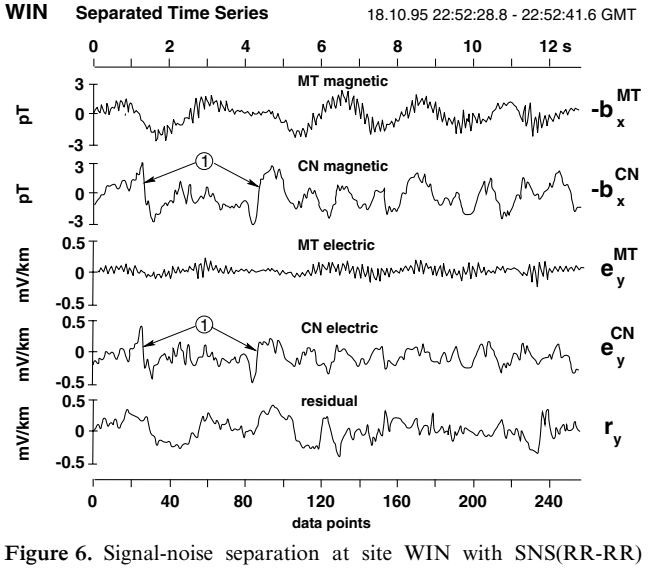

Figure 6. Signal-noise separation at site WIN with SNS(RR-RR) method in time domain for one section. From top to bottom: MT magnetic signal $-b_x^{MT}$, CN magnetic signal $-b_x^{CN}$, MT electric signal e_y^{MT}, CN electric signal e_y^{CN} and residual r_y. For easier comparison magnetic time-series are inverted. The circled 1 indicates signals from inspection measurements along a pipeline.

During one week we recorded strong rectangular noise signals which were caused by inspection measurements along a pipeline near the town of Rochlitz at the northern boundary of the Granulite Massif. At the location KIE we observed the pipeline noise mainly in the north magnetic variations and in both north and east electric components. Fig. 7 shows the time-series for the east electric component. The test voltage is switched on for 3 s and then switched off for 27 s. The CN signals in both the magnetic and electric variations are 2–3 magnitudes larger than the MT signals. Compared with the MT signals, a considerable part of the CN signal remains in the residual and the signal separation is not completely successful. Perhaps additional noise signals with other transfer characteristics are not separated. Nevertheless, for periods of less than 10 s we were able to reproduce the 'true' transfer function (estimated from time-series without pipeline noise). The pipeline noise transfer function is very well determined (Fig. 8). The apparent resistivities rise from 1000 Ω m ($T=10^{-1}$ s) to 10^6 Ω m ($T=10$ s) and the phase is small (about -180°). This results show that the pipeline noise can be described with the model of an electric dipole.

5 SIGNAL SEPARATION FOR PERIODS GREATER THAN 5 s

For periods from 5 to 200 s we used a bandpass filter and decimated the original data (sampling rate 20 Hz) by a factor 64 (Wight & Bostick 1980). We show results from site KIE near the northern boundary of the exposed Saxonian granulites. The 'true' transfer function for site KIE is well determined from data sections with low noise level from Oettinger (1999). We focus on the transfer functions derived from 114 noisy data sections from 1995, October 1 and 2.

As remote time-series we used the magnetic and electric variations at site GAN (350 km away). The separation transfer function is estimated with the RR method. Apart from the smallest periods, the element T_{yy} is well determined (Fig. 9). The roughness of the smallest periods is caused by a low coherency squared between the measured and predicted magnetic variations (Fig. 9c).

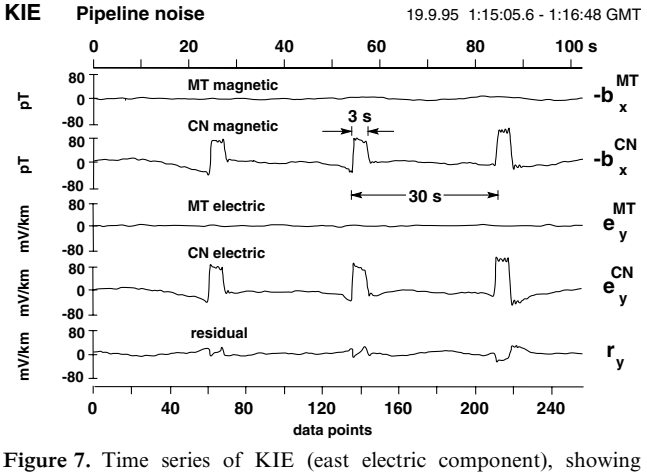

Figure 7. Time series of KIE (east electric component), showing strong noise signals caused by inspection measurements (corrosion protection) along a pipeline. Notation as in Fig. 6 but for time-series length 102.4 s

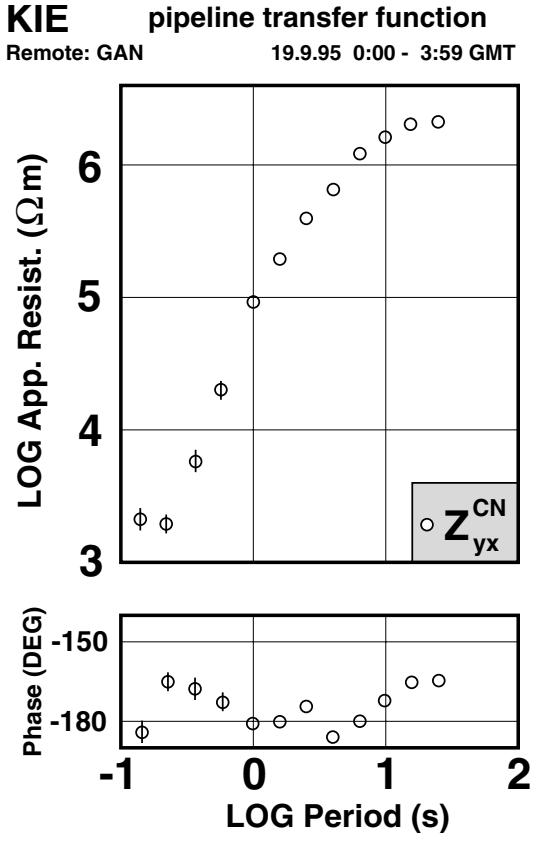

Figure 8. Pipeline-noise transfer function Z^{CN}_{yx} caused by rectangular voltage signals from inspection measurements along a nearby pipeline.

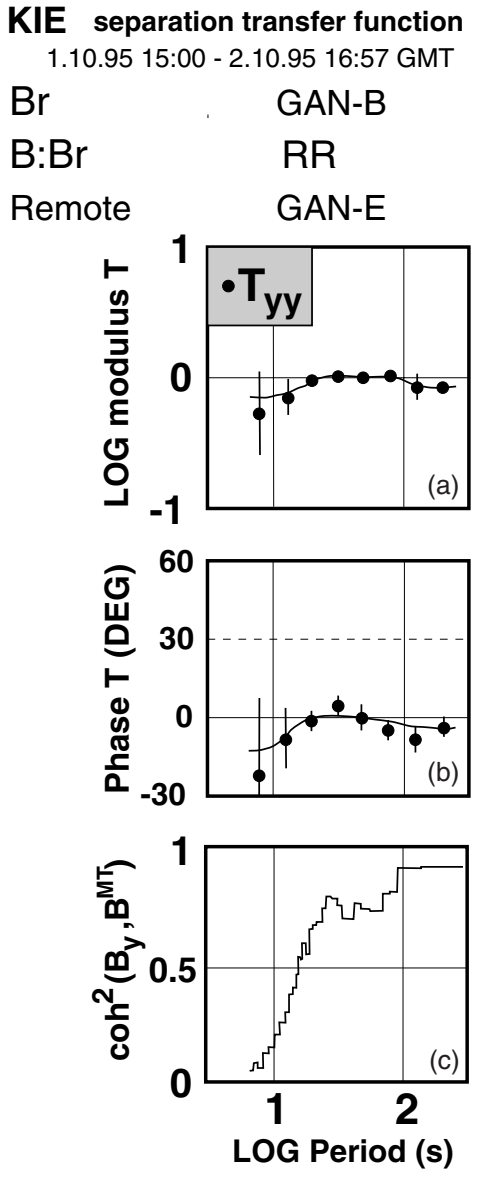

Figure 9. (a) separation transfer function T_{yy} between the east components of the magnetic variations at site KIE and the remote site GAN (dots: band-averaged values, lines: smooth transfer functions). (c) associated coherence-squared. For RR estimates electric variations at site GAN were used.

Fig. 10 shows different estimates for the MT and CN transfer function at site KIE. The comparison with the 'true' transfer function (broken line) shows that the LS method gives completely wrong results and the RR method yields unstable values. With the SNS(RR-LS) method we were able to reproduce the 'true' function, but with some larger errors for the small periods. The partial coherence-squared is 0.07 between the electric and MT magnetic variations and 0.14 between the electric and CN magnetic variations. Hence, the CN signals are larger than the MT signals and dominate this recording. Therefore the LS estimates have a similar appearance to the CN transfer function (open circles). However, the main part of the measured variations consists of uncorrelated noise. This does not influence the transfer function estimation because the signal separation is successful.

Fig. 11 shows the time-series for one section (length 13.65 min). The high amplitudes in the residual demonstrate the large share of uncorrelated noise in the electric field. The CN magnetic variations are at times much larger than the MT magnetic variations. The sinusoidal-like noise signal between the time marks 2 and 7 min (shaded) have the appearance of a natural MT signal, but the comparison with simultaneously recorded magnetic noise signals from other locations along the profile show that the classification as noise is correct. Fig. 12 gives the magnetic noise signals for the same time interval at the locations KIE (questionable variations shaded), KON and DIB. The noise signals in the east component of all three sites are highly coherent (especially in the shaded interval between the 2 and 7 min), but the amplitudes are very different (large scaled at sites DIB and KON). It turned out that these kind of signals were the most dominant noise signals in the Granulite Massif. The signals were especially strong at locations near the NS running electrified railway track Döbeln–Chemnitz (Oettinger 1999). They appear more often during day time and in the magnetic east component. Therefore we assume that the strong noise signals were caused by trains (leakage currents caused by acceleration processes). At the sites near the train-track the CN transfer functions have phases of $\pm 90^\circ$ (Oettinger 1999).

6 CONCLUSIONS

To derive useful MT impedance tensors from time-series which are contaminated by large and continuous correlated noise it is valuable to separate the time-series into MT signal and correlated noise parts. This requires a clean remote site (for

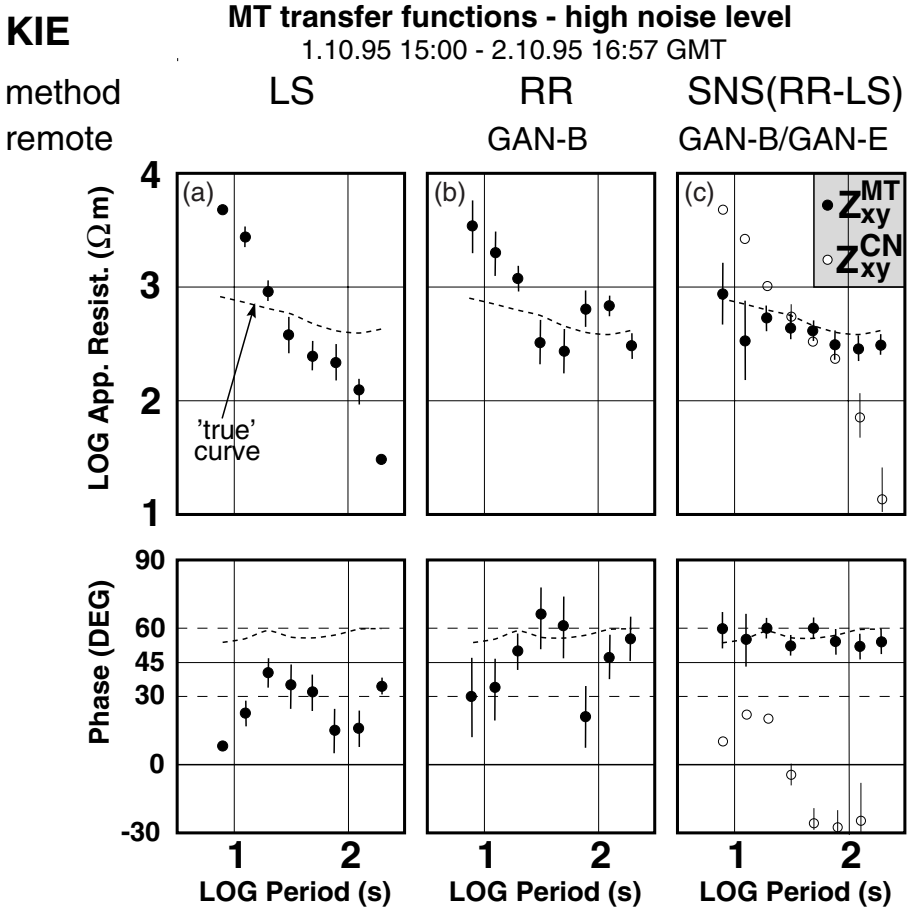

Figure 10. Different estimates of the MT transfer function Z^{MT}_{xy} (dots) at site KIE, derived from 114 sections with high noise level. (a) LS method, (b) RR method, (c) SNS(RR-LS) method. Open circles: CN transfer function Z^{CN}_{xy}. Dashed line: 'true' transfer function (Oettinger 1999). Remote site: GAN (350 km away).

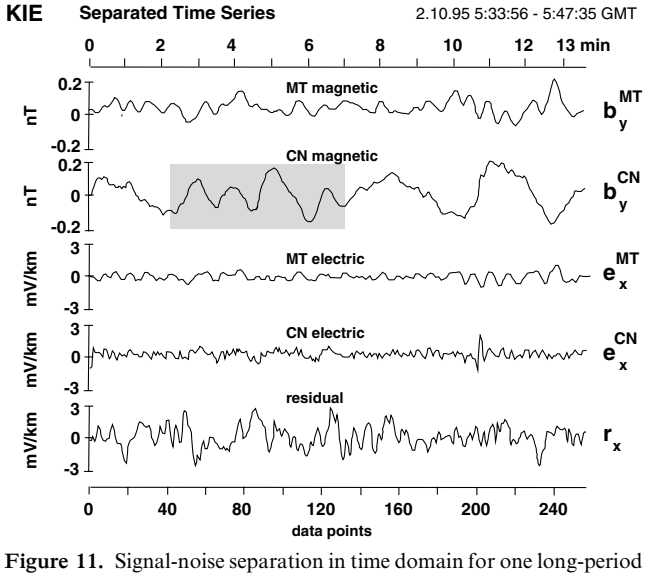

Figure 11. Signal-noise separation in time domain for one long-period data segment at site KIE. From top to bottom: MT magnetic signal b^{MT}_y, CN magnetic signal b^{CN}_y, MT electric signal e^{MT}_x, CN electric signal e^{CN}_x and residual r_x. Shaded area: correlated noise identified also at neighboring locations, see Fig. 12

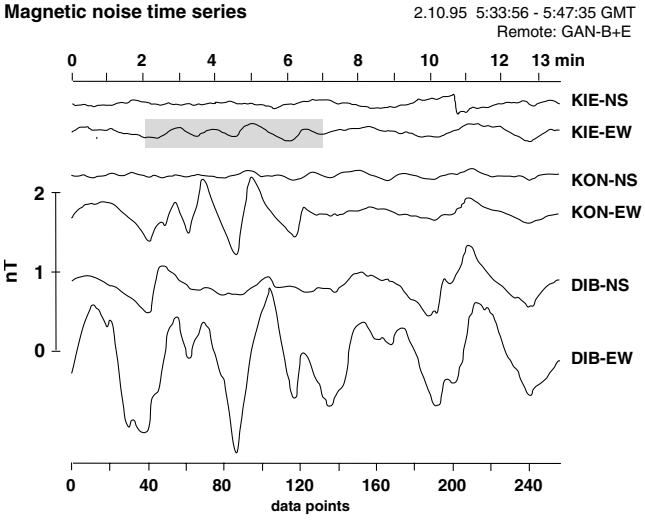

Figure 12. Simultaneously recorded magnetic noise signals at the sites KIE, KON and DIB. Signal separation is done with SNS(RR-LS) method using remote magnetic and electric time-series from site GAN (350 km away). The shaded area denotes the same noise signals as shown in Fig. 11.

the signal–noise separation method) or two remote sites, which contain uncorrelated noise (for the signal–noise separation remote-reference method).

MT time-series from the Saxonian Granulite Massif (East Germany) contain different levels of correlated and uncorrelated noise. The processing results based on signal–noise separation show that only 10 per cent or even less MT signal in the measured time-series are sufficient to derive realistic MT transfer functions. Because all remote data sets contain uncorrelated noise, the quality of the signal separation was improved by using a second remote data set. Most noise sources in the Saxonian Granulite Massif can be described by a model of a grounded electric dipole. If there is a dominant noise source, the accompanying noise transfer function is well determined, for example square wave pulses from inspection measurements along a pipeline.

For periods greater than 5 s the time-series in Saxonia contain correlated noise signals which can be measured over distances of some tens of kilometres. These noise signals are at times much larger than the MT signals and were probably caused by electric trains. For signal separation it was necessary to use remote data which was recorded 350 km away. For short periods from 0.1 to 5 s nearby remote sites (distance 5 km) were also suitable.

The results of this paper demonstrate the importance of low-noise reference stations far away from the local profile. In highly industrialized regions like Saxonia one can only derive high quality MT impedance tensors with help of suitable remote data. For further campaigns special care should be taken to run reference stations in an appropriate place.

ACKNOWLEDGMENTS

We gratefully acknowledge the funding of our research, which was provided by the German Science Foundation (DFG) through the Priority Research Programme 'Orogenic Processes' (projects Ha1210/19, Pr74/17-3,-4). We appreciate the thoughtful comments by our colleague Andreas Müller. We also appreciate the comments of the two unknown reviewers and of Karsten Bahr which amended the manuscript considerably. Numerous students and scientists from the University of Leipzig are thanked for help during the field campaign.

REFERENCES

Banks, R., 1998. The effects of non-stationary noise on electromagnetic response estimates, *Geophys. J. Int.,* **135,** 553–563.

Chave, A. & Thomson, D., 1989. Some comments on magnetotelluric response function estimation, *J. geophys. Res.,* **94,** 14 215–14 225.

DEKORP & Orogenic Processes Working Groups, 1999. Structure of the Saxonian Granulites: geological and geophysical constraints on the exhumation of high-pressure/high-temperature rocks in the mid-European Variscan belt, *Tectonics,* **18,** 756–773.

Egbert, G.D., 1997. Robust multiple-station magnetotelluric data processing, *Geophys. J. Int.,* **130,** 475–496.

Egbert, G.D. & Booker, J.R., 1986. Robust estimation of geomagnetic transfer functions, *Geophys. J. R. astr. Soc.,* **87,** 173–194.

Gamble, T., Goubau, W. & Clarke, J., 1979. Magnetotellurics with a remote reference, *Geophysics,* **44,** 53–68.

Goubau, W., Gamble, T. & Clarke, J., 1978. Magnetotelluric data analysis: removal of bias, *Geophysics,* **43,** 1157–1166.

Jones, A., Chave, A., Egbert, G., Auld, D. & Bahr, K., 1989. A comparison of techniques for magnetotelluric response function estimation, *J. geophys. Res.,* **94,** 14 201–14 213.

Junge, A., 1996. Characterization of and correction for cultural noise, *Surv. Geophys.,* **17,** 361–391.

Krawczyk, C., 1999. Constraints on distribution and exhumation of high-pressure rocks from geophysical studies—the Saxothuringian case between Bray Fault and Elbe Linie, in *Orogenic Processes—Quantification and Modeling in the Variscan Belt of Central Europe,* eds Franke, W., Haak, V. & Oncken, O., *Geol. Soc. Lond. Spec. Publ.,* **179,** 303–322.

Larsen, J. C., Mackie, R. L., Manzella, A., Fiordelisi, A., Rieven, S., 1996. Robust smooth magnetotelluric transfer functions, *Geophys. J. Int.,* **124,** 801–819.

Michel, J., 1997. Datenverarbeitung einer Magnetotellurik-Messung im Odenwald, *M.Sc. thesis,* Institut für Geophysik und Meterologie der Universität zu Köln, Cologne.

Michel, J. & Tezkan, B., 1996. Prozessing von Magnetotellurik-Daten aus dem Odenwald, in *16. Kolloquium Elektromagnetische Tiefenforschung, Burg Ludwigstein, 9.12.4.1996*, pp. 162–166, ed. Bahr, K. & Junge, A., DGG.

Müller, A., 2000. A new method to compensate for bias in magnetotellurics, *Geophys. J. Int.,* **142,** 257–269.

Oettinger, G., 1999. Magnetotellurische messungen im sächsischen granulitgebirge: separation von nutz- und störsignalen und verteilung der elektrischen leitfähigkeit, *Ph.D. thesis,* Freie Universität Berlin, Scientific Technical Report STR99/21, GeoForschungsZentrum Potsdam.

Polk, C., 1982. Schumann resonances, *Handbook of Atmospherics,* Vol. 1, pp. 111–178, ed. Volland, H., CRC Press, Boca Raton, FL.

Ritter, O., Junge, A. & Dawes, G.J.K., 1998. New equipment and processing for magnetotelluric remote reference observations, *Geophys. J. Int.,* **132,** 535–548.

Schmucker, U., 1984. EM Übertragungsfunktionen aus Beobachtungen mit mehreren gleichzeitig registrierenden Stationen, in *10. Kolloquium Elektromagnetische Tiefenforschung, Grafrath in Oberbayern,* pp. 35–36, eds Haak, V. & Homilius, J., Free University, Berlin.

Sims, W., Bostick, F., Smith, H., 1971. The estimation of magnetotelluric impedance tensor elements from measured data, *Geophysics,* **36,** 938–942.

Szarka, L., 1988. Geophysical aspects of manmade electromagnetic noise in the earth—a review, *Surv. Geophys.,* **9,** 287–318.

Wight, D. & Bostick, F., 1980. Cascade decimation—a technique for real time estimation of power spectra, *Proc. IEEE Int. Conf. Acoustic,* pp. 626–629.

Zonge, K. L. & Hughes, L. J., 1987. Controlled source audio-frequency magnetotellurics, in *Electromagnetic Methods in Applied Geophysics. Applications,* pp. 713–809, ed. Nabighian, M.N., SEG, Tulsa.